Interaction of Miltefosine with Microcavity Supported Lipid Membrane: Biophysical insights from electrochemical impedance spectroscopy

Nirod Kumar Sarangi, Amrutha Prabhakaran, Tia E. Keyes*

School of Chemical Sciences and National Centre for Sensor Research, Dublin City University, DCU Glasnevin Campus, Dublin 9, D09 W6Y4, Ireland

* e-mail: tia.keyes@dcu.ie

Abstract

Miltefosine an alkylphosphocholine analogue, is the only drug taken orally for the treatment of leishmaniasis-a parasitic disease caused by sandflies. Although it is believed that Miltefosine exerts its activity by acting at the lipid membrane, detailed understanding of the interaction of this drug with eukaryotic membranes is still lacking. Herein, we exploit microcavity pore suspended lipid bilayers (MSLBs) as a biomimetic platform in combination with a highly sensitive label-free electrochemical impedance spectroscopy (EIS) technique to gain biophysical insight into the interaction of Miltefosine with host cell membrane as a function of lipid membranes composition. Four membrane compositions with increasing complexity were evaluated; DOPC, DOPC:Chol (75:25), domain forming DOPC:SM:Chol (40:40:20) and mammalian plasma membrane (MPM) mimetic DOPC:DOPE:Chol:SM:DOPS (32:25:20:15:8) and used to study the interaction of Miltefosine in a concentration-dependent manner using EIS. The membrane resistance changes in response to Miltefosine were modelled by an empirical Langmuir isotherm binding model to provide estimates of binding saturation and equilibrium association constant. Miltefosine was found to have greatest impact on electrochemical properties of the simpler membrane systems; DOPC and DOPC:Chol, where these membranes were found to be more susceptible to membrane thinning, attributed to strong permeation/penetration of the drug whilst, compositions that included both Chol and SM, expected to contain large liquid-ordered domains exhibited weaker changes to membrane resistance but strongest drug association. In contrast, at the MPM membrane, Miltefosine exerts weakest association, which is tentatively attributed to electrostatic effects from the anionic DOPS but some membrane thinning is observed reflected in change in resistance and capacitance values attributed to some weak permeation.

Keywords: pore-suspended bio-membranes, impedance spectroscopy, lipid-drug interaction, leishmaniasis, Miltefosine, drug-permeation

DOI: 10.1002/elan.((will be filled in by the editorial sttaff))

1. Introduction

Leishmaniasis diseases in humans are caused by intracellular protozoan parasites of the species *Leishmania*. They are spread by the bite of sandflies, and lead to numerous symptoms including skin ulceration, low red blood cells count, and enlarged spleen and liver.[1,2] Miltefosine is an alkyl phospholipid analogue used in the past for its antitumor[3] and anticancer activity[4], and the only oral drug currently approved for the treatment of leishmaniasis.[5–7] The drug acts on *Leishmania* primarily by affecting amastigote and promastigote stages of the species.[8] It is widely believed that Miltefosine exerts its activity through interaction with the parasite cell membrane surface[9], inhibiting cytochrome C oxidase and causing apoptosis-like cell death through its modification of membrane integrity.[10] Although the clinical efficacy of Miltefosine is well established along with its pharmacology and therapeutic efficiency[11,12], the molecular mechanism of its interaction at the lipid bilayer membrane, where its action is centred, is not fully elucidated. Given it is an alkyl phospholipid, it assembles readily into the cell membrane where it accumulates and interferes with membrane based signalling. Data from cell (macrophages) based studies show Miltefosine affects lipid homeostasis, autophagy, and dampening NLRP3 inflammasome assembly.[13] Furthermore, it is transported across the cell membrane, but details of the mechanism i.e.

whether by passive or active mode remain unclear. In this context, model membrane studies can be a useful platform to provide molecular-level insight towards the Miltefosine action.

Two widely applied surrogate technologies for *in vitro* prediction of passive small molecule membrane permeability, that have been applied to study of Miltefosine are parallel artificial membrane permeability assay (PAMPA)[14,15] and the immobilized artificial membrane (IAM)[16]. These methods have the advantage of being relatively straightforward to implement and are advances on LogP/D studies where they provide reliable insight into drug physicochemical properties, but are limited in that they do not present a true lipid membrane for analysis. Langmuir monolayers at the air/water interface have been examined and Miltefosine binding to individual phospholipids and cholesterol has been reported at these monolayer films.[17–19] The mechanism of Miltefosine adsorption was investigated in detail by Ménez et al.[20,21] using another *in vitro* permeability testing caco-2 cells assay. From these studies, it was observed that below 50 μM concentration, membrane translocation was found to be mediated mainly by non-saturable passive paracellular diffusion, while above this concentration, the transport mechanism is saturable and is likely an active carrier-mediated cellular transport. Although the above studies provide important insights into Miltefosine transport, possible inhibition due to the transporter protein present in caco-2 cell line which could result in drug-drug interactions, use of high concentration of drug above physiological concentration (typically <20 μM)[11,22] and importantly, the above method is time-consuming and individual membrane role towards the drug binding, etc limiting its use.

True lipid bilayer membranes provide a useful *in vitro* approach to modelling membrane interactions and include microcavity supported lipid bilayers (MSLBs) described herein. They offer low cost, but strongly biomimetic means to study the interactions of drugs with lipid bilayer during the earliest stages of drug development.[23] MSLBs are one out of several *in vitro* platforms that have been used to anticipate passive membrane permeability and membrane-associated toxicological problems isolated from the complexity of the living cell.[24–27] Other true lipid bilayer models such as liposomes and supported lipid bilayers (SLB) have been widely applied to interrogate the interaction of membrane lipids with small molecules.[28–33]

For drugs like Miltefosine, their study by surrogate methods such as PAMPA, or in biophysical models such as liposomes, that use optical detection, is a challenge because such drugs do not contain an accessible luminophore or chromophore, and their strong structural analogy to lipids renders them difficult to distinguish from background using vibrational spectroscopic methods.

Interrogation by electrochemical means then, becomes a valuable alternative for evaluating drugs without chromophores. Liposomes are difficult to interrogate, electrochemically but supported lipid bilayers are assembled at interfacial supports that can be readily addressed by electrochemistry and indeed surface-enhanced vibrational spectroscopy[29,34–38]. Though SLBs suffer from artefactual effects of pinning on the fluidity and functionality of the bilayer and associated proteins that can limit biomimicry of SLBs.[39–41] Several modifications have been introduced to decouple the proximal leaflet from the substrate and promote the mobility of membrane. These include tethered lipid bilayer membranes and cushioned bilayer membranes[40,42–46] but issues as described, over mobility and also over lack of receptor volume for drug permeation studies remained an issue.

Lipid membranes supported over aqueous filled pores provide a strongly biomimetic approach to overcome these issues whilst maintaining membrane stability. Most importantly, in the case of buffer filled pore supported bilayers, they offer the advantage of receiver aqueous reservoir, that SLBs lack, in contact with proximal leaflet, that mimics the cytoplasm.[47–50] We recently reported such microcavity array supported lipid bilayers (MSLB) formed on the gold substrate and applied as working electrodes for electrochemical measurements to study drug-membrane and protein-membrane interaction.[36,51–54]

Herein, we use the MSLB platform, to study electrochemical impedance spectroscopic response of biomembrane on Miltefosine drug incubation with four different symmetric biomembranes composed of DOPC, DOPC:Chol (75:25), DOPC:SM:Chol (40:40:20) and mammalian plasma membrane (MPM) mimetic. Of the four, the first three mimic the eukaryotic membranes with varied complexity, whereas the last one is a mammalian mimetic fusogenic composition (MPM) comprised of 32% DOPC, 25% DOPE, 20% cholesterol, 15% SM and 8% DOPS coined 'nature's own' by Lentz et al[55] is intended as a mimic of the gastrointestinal tract. The concentration of Miltefosine at each membrane type was varied systematically within a physiological concentration range[11] in PBS buffer and the impact of Miltefosine on the electrical properties of these membranes were examined. Changes to the membrane resistance and capacitance plotted using an empirical Langmuir isotherm binding model provide quantitative insights into relative extent of membrane responses towards Miltefosine interaction.

2. Materials and Methods

2.1. Materials

1,2-Dioleyl-*sn*-glycerophosphocholine (DOPC), 1,2-Dioleyl-*sn*-glycerophosphoethanolamine (DOPE), 1,2-Dioleyl-*sn*-glycerophosphoserine (DOPS), 1,2-Dioleyl-sn-glycerophosphoglycerol (DOPG) and Sphingomyelin (Brain, Porcine) in powder form were purchased from Avanti polar lipids (Instruchemie, The Netherlands). Cholesterol, Miltefosine and phosphate buffer saline (PBS) tablets were purchased from Sigma-Aldrich (Wicklow, Ireland). Ultrapure water with a resistivity ≥ 18.2 MΩcm was produced by a Milli-Q (Millipore Academic) system and used for monolayer studies and buffer preparation. All reagents were of high purity and obtained from Sigma-Aldrich.
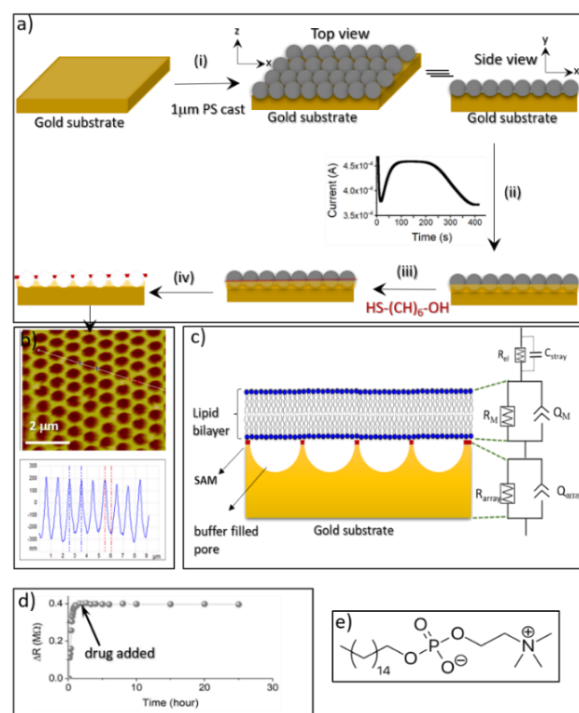
2.2. Methods

2.2.1. Fabrication of microcavity array substrate

The fabrication of microcavity array on the gold substrate was completed with a slight modification of the procedure reported previously.[36] A step-by-step method for the fabrication of cavity array is shown in Scheme 1. First, in step-i, the calculated amount of 1 µm polystyrene (PS) sphere (1 wt % v/v in Milli-Q water) was drop cast onto the cleaned gold substrate of size 1.5×1 cm². The PS solutions were left for drying overnight in a closed chamber at 4 °C, while keeping the slide at a slanted angle to ensure monolayer coverage of the PS spheres across the whole area. In step-ii, PS covered gold substrate was subjected to gold deposition by submerging the substrate into gold electroplating solution. The controlled gold deposition was carried out using chronoamperometry. The deposition was monitored from the shape of the *I*-t curve. The growth process was continued until the gold deposition reached the equator of the hexagonally packing array PS templating spheres and was then stopped. This takes approximately 400 s as shown from the *I*-t curve in Scheme 1a, step-ii. Following gold deposition, in step-iii, the electrode was washed with Milli-Q water, dried under a gentle stream of N₂ gas, and immersed in 1 mM ethanolic solution of 6-mercapto-1-hexanol for 48 hours, to form self assembled monolayer (SAM) at the exposed gold surface. After 48 hours, the gold substrate was removed and washed in a copious amount of ethanol to remove excess unbound thiol. Finally, in step-iv, the substrate was soaked in THF for 5 min to remove the PS template and a gold microcavity array with thiol SAM localized to the top inter-pore gold surface is formed. As described previously, retention of the templating PS sphere until the last step prevents the SAM forming at the pore interior, limiting SAM to the regions at the top surface of the array between pores.[52] Using this approach our SAM comprised an alkanethiol molecule with terminal hydroxyl group that

serves to increase surface hydrophilicity promoting stable bilayer formation whilst leaving the interior cavity for aqueous buffer filling or selective chemical modification of other functional groups. The cavities used herein are of 1 µm radius and 0.5 µm pore depth, confirmed by atomic force microscopy (Scheme 1b).

2.2.2. Fabrication of pore suspended lipid bilayer

The thiol modified gold substrate with terminal -OH group promotes the wettability of gold substrate and renders it suitable for Y-type Langmuir-Blodgett transfer of monolayer. Crucially, immediately prior LB deposition, the cavities were filled with aqueous PBS buffer. Following filling, the gold substrate was submerged into a Langmuir trough (model KN2006 from KSV-Nima technology) filled with Milli-Q water for LB deposition at the air/water interface.

Scheme 1. (a) Schematic representation of microcavity array using polystyrene template method. (b) Illustrates AFM image (*Top*) and line profile analysis (*bottom*) of gold microcavity array. The scale bar in the image was 2 µm. (c) Represents a schematic representation of MSLB (*left*) along with ECM circuit (*right*). Various components of the ECM are; R_{el} : electrolyte resistance, C_{stray}: stray capacitance, R_M: membrane resistance, Q_M: membrane capacitance, R_{array}: cavity array resistance, and Q_{array}: array capacitance. (d) Representative stability plot of DOPC MSLB showing the relative change in resistance versus time. An arrow mark is to show the equilibration time (~2 hr) at which Miltefosine is added to the cell. (e) Chemical structure of hexadecylphosphocholine, Miltefosine.

Next, approximately 50 µL of 1 mg/mL the lipid solution (either single component or lipid mixtures with required mole ratios) were prepared in chloroform and added to the water surface dropwise. Fifteen minutes were allowed for the evaporation of chloroform before lipid monolayer compression. The rate of compression was set for 9.8 $Å^2$molecule^{-1}min^{-1} using software control and, typically two compression and two expansion cycles were performed before the collapse surface pressure reached. The surface pressure of the lipid monolayer due to the reduction of surface tension of water was monitored using a Pt Wilhelmy plate sensor. Next, the monolayer is compressed up to 33 mN/m, and held for 5 mins. The first monolayer was transferred by vertically withdrawing the substrate from the monolayer at a speed of 5 mm/min (up-stroke) and the second layer was formed by bringing the substrate via down-stroke at a speed of 3 mm/min to the monolayer covered aqueous subphase, to form the microcavity suspended lipid bilayer (MSLB). A schematic representation of the MSLB is shown in Scheme 1c. Finally, the substrate was removed from the water subphase without exposure to air and transferred to the electrochemical cell for measurement.

2.2.3. Electrochemical impedance spectroscopy

Electrochemical impedance spectroscopy (EIS) measurement was performed with a CHI760e (CH Instrument, USA). A standard 3-electrode cell was employed for all measurements, comprised of gold microcavity array covered lipid bilayer as a working electrode, an Ag/AgCl (1 M KCl) reference and a coiled platinum wire counter electrode. The EIS data were recorded across a frequency range of 0.05 to 10^5 Hz with an AC modulation amplitude of 10 mV at a DC potential bias of 0 V (vs Ag/AgCl). All measurements were carried out in a glass cell (approximate volume of 4 mL of 0.01 M PBS). The EIS of the aqueous filled microcavity array coated with the lipid bilayer was measured initially before the addition of drugs to ensure signal stability. The non-Faradaic EIS signal from the MSLBs was evaluated for stability, and was found that when initially placed in contact with the PBS buffer, an initial fluctuation of resistance is seen that stabilizes within an hour and then remains unchanged over a prolonged window ~24 hrs (Scheme 1d). This 24 hrs window of stability is well beyond our experimental time window (3-4 hrs) for Miltefosine binding studies. A time lag of 90-120 mins was allowed for each membrane composition to ensure it had equilibrated in the electrochemical cell (no fluctuation of EIS) before drug solutions were titrated. The EIS response of the lipid bilayer was then measured at incremental drug concentration over the range 0-20 µM. The Miltefosine (see chemical structure in Scheme 1e) was

initially prepared as a stock solution (10 mg/mL) in PBS and this was aliquoted into the cell to achieve the required final drug concentration and mixed thoroughly. At no point, did the volume added to the cell exceed 20 µL. An equilibration time of 20 mins was allowed after each aliquot before the data were recorded. Each measurement takes approximately 3 min to complete and was carried out at room temperature (22±1 °C). At least, 6-8 runs (20-30 mins) were performed for each concentration to ensure an equilibrated signal of impedance. The impedance of the MSLBs at each composition was assessed in triplicate, as well as their temporal stability. The measured data were analyzed using Z-View software (Scribner Associates, v3.4e) with the fitting equivalent circuit model (ECM) shown in Scheme 1c. The best fit using the ECM circuit was assessed from both from visual inspection of the fit residuals and from $χ^2$, typically < 0.001.

3. Results and Discussion

The fabrication of microcavity pore array across a ~1×1 cm^2 gold electrode was achieved via controlled gold electrodeposition through polystyrene sphere template as previously described by us.[36,51–54] Following the fabrication of micropore array, the SAM modified electrodes were applied to layer by layer transfer of two lipid monolayers using the LB method to form the final MSLB. A schematic representation of the MSLB is shown in Scheme 1c. Non-Faradaic EIS was employed to monitor the membrane electrical properties. A representative Nyquist trace of the EIS signal for DOPC MSLB is shown in Fig. 1a (open square). The Nyquist trace represents the sum of real (Z′) and imaginary (Z″) components of the complex impedance, which originate from the resistance and capacitance of the cell. The non-Faradaic Nyquist trace shifts towards Z″ (y-axis), indicating an increase in impedance of the membrane. Similarly, a shift towards Z′ (x-axis) implies that the impedance is decreased. In addition, the capacitive properties can be visualized from the angular frequency normalized complex capacitance plot as shown in Fig. 1b for DOPC membrane (open square). A representative EIS plot of the cavity array electrode prior to bilayer fabrication is shown in Fig.1 (open circle). From both the Z′ vs, -Z″ and Y′/ω vs. Y″/ω plots, it is clear that DOPC successfully spanned across the cavity array, reflected from an increase in impedance and decrease in capacitance behaviour respectively. The Bode plot shows the phase angle changes within different frequency ranges, 0.05 Hz to10^5 Hz (Fig. 1a, *inset*). To gain quantitative estimation of membrane resistance and capacitance changes, the EIS data was fit to an equivalent circuit model (ECM), (solid lines in Fig. 1) using a heuristic approach for the MSLB[54] as shown in Scheme 1c. The circuit applied, consists of three parallel

components connected in series; a solution electrolyte resistance which is parallel to the stray capacitance (R_{el}, C_{stray}), in series with a resister and a constant phase element (CPE), which are in parallel, and corresponds to the electric and dielectric properties of the lipid membrane deposited on the electrode surface (R_M, Q_M), and, which is further connected in series with a resistor and CPE, which are also parallel and corresponds to the resistance and dielectric properties of cavity array (R_{array}, Q_{array}). Note, in the ECM, C_{stray} component accounts for the capacitance associated with cable, connector, or electrochemical cell, typically in the order of ~nF. From the fit, R_{array} and Q_{array} remain largely unchanged with drug titration and were found typically in the range of ~50-60 µF·s^{m-1} and ~10 kΩ respectively. In a control measurement while titrating the drug in our cavity platform prior to bilayer formation, we did not observe any change in impedance signal (data not shown) suggesting that the Miltefosine did not adsorb to the surface of gold. A CPE (Q) is used in the ECM instead of a pure capacitor (C) as the impedance of our working electrodes usually deviates from pure capacitor due to microscopic chemical inhomogeneity associated with both the porous electrode and the bilayer membrane. The complex impedance of a CPE is given by the following equation (1);

$$CPE = 1/Q(j\omega)^m \qquad (1)$$

where Q is analogous to the magnitude of the capacitance, ω is the angular frequency expressed in rad/s, and m is a real number between 1 and 0. When m approaches 0, the CPE behaves like a pure resistor and when $m = 1$, the CPE behaves as an ideal capacitor. Typically, in our system, we observed and m value close to 0.5 for Q_{array} meaning the CPE becomes a series RC circuit or Warburg impedance, and was found to be $m \approx 0.93$ for membrane. Note that for the CPE, Q has a unit that depends on the value of m (e.g. µF·s^{m-1}) rather than true capacitance units of µF. While a true membrane capacitance (C_M) can be estimated from the Q_M value using the expression $C_M(\omega) = Q_M\omega^{m-1}$, it only holds true for a specific ω, limited to the specific ECM[56] and so is not used in the present work. We focus instead on the relative changes to membrane capacitance and resistance upon drug interaction throughout this work. Furthermore, the R_M and Q_M values are not normalized to the surface area. This is because the sphere templating method used for fabrication leads to some variation in electrode area from the substrate to substrate due to variation and discontinuity in PS sphere packing during template formation (typically <2-5% of 1×1 cm² gold substrates show such discontinuity). This can in turn affect SAM coverage. We, therefore, quote the relative change (Δ) in resistance and capacitance values from the initial values for the pristine bilayer absolute

resistance for each substrate. The relative changes to membrane resistance (ΔR) and capacitance (ΔQ) is defined as ($R_M^0 - R_M^{drug}$) and ($Q_M^0 - Q_M^{drug}$); where R_M^0 and Q_M^0 represents respectively the membrane resistance and capacitance in the absence of drug, and R_M^{drug} and Q_M^{drug} are the respective values when the drug is present in the contact solution. Across replicate platforms, the absolute resistance of the membranes are closely replicated and of the order of DOPC:SM:Chol > MPM > DOPC:Chol > DOPC typically in the range ~1-6 MΩ and CPE values are at 6-8 µF·s^{m-1} and this trend confirm to our previous report.[54]
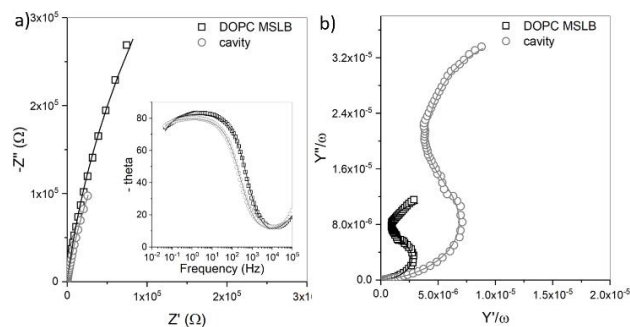

Fig. 1. a) Nyquist plot and b) frequency normalized complex capacitance plot obtained during impedance measurement at cavity array (open circle, ○) and DOPC MSLB (open square, □). (*inset* in a) Represents Bode plot (frequency vs phase angle, theta). In each panel, for DOPC MSLB, solid lines represent the fit using ECM, shown in Scheme 1c, and for cavity, the parallel component (R_M and CPE$_M$) was omitted from the circuit. EIS measurements were performed in 0.01 M PBS buffer within the frequency ranges between 0.05 Hz to 10⁵ Hz at 0 V DC bias potential vs Ag/AgCl (1 M KCl) with an AC amplitude of 10 mV at 22±1°C. A three-electrode set-up where gold cavity/MSLB, Ag/AgCl (1M KCl) and Pt coiled served as working, reference and counter electrode respectively.

To provide insight into the relative changes in membrane resistance and capacitance, a drug concentration-dependent study was investigated. A range of concentrations of Miltefosine e.g. to a final concentration of 1, 5, 10, and 20 µM was titrated to each membrane type and the EIS measured. Each assay was repeated a minimum of 3 times on a fresh substrate. Representative drug titration data are shown in Figure 2. In addition, representative Bode plots for the drug titration data at DOPC membrane is presented in Fig. S1 (SI). From visual inspection of the Nyquist trace, the shift of impedance curve towards Z′-axis for the DOPC membrane occurs at 1 µM Miltefosine. While, upon increasing the concentration further, the shift reverts back toward impedance of the pristine membrane i.e., towards -Z″-axis (Fig.2a). For DOPC:Chol membrane, a systematic shift of Nyquist trace toward Z′-axis is observed with increasing

drug concentration. The absolute magnitude of the changes are greater than DOPC membranes suggesting the condensing effect of cholesterol on the DOPC offers some protection to the membrane against loss of packing integrity (Fig. 2b).

In contrast, for the domain-forming membranes explored, DOPC:SM:Chol (Fig. 2c) and MPM (Fig. 2d), the changes to the impedance plots are not as significant as those for DOPC and DOPC:Chol membrane, indicating weaker extent of change to membrane admittance, which is likely consistent with tighter packing of the membranes containing both Chol and SM.[52,54].

To gain quantitive insight, all the EIS data in absence or presence of Miltefosine at different concentrations were fit to the ECM model shown in Scheme 1 and relative resistance and capacitance changes to the membrane
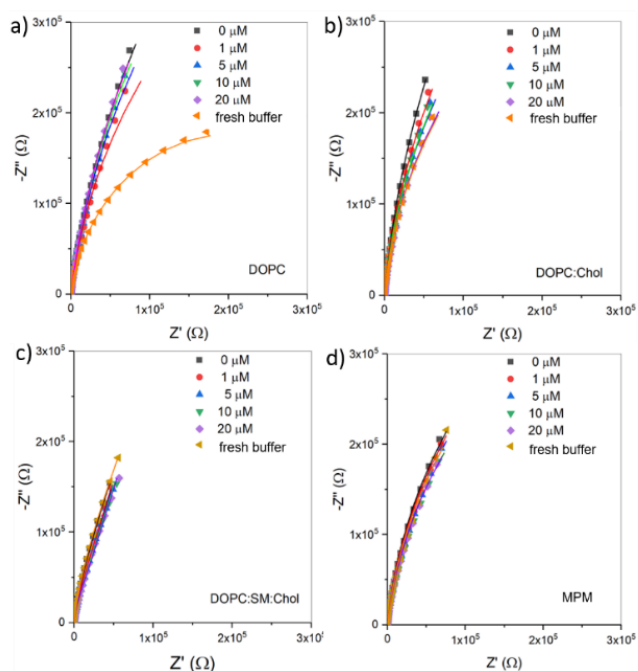
Miltefosine and are shown in Fig. 3 a and b respectively. The data are tabulated in Table 1 and Table 2 respectively. As expected, based on the Nyquist plots, the magnitude of the changes in resistance values in response to exposure of Miltefosine are greater for the DOPC and DOPC:Chol membranes compared with DOPC:SM:Chol and MPM compositions (Fig. 3a). Unlike resistance change, the change in capacitance values across all concentrations of Miltefosine varied differently as reflected in Fig. 3b. The increase in capacitance is observed for DOPC, DOPC:Chol and MPM compositions, whereas for DOPC:SM:Chol membrane, Miltefosine induces a decrease in capacitance. Nonetheless, at lower concentrations of Miltefosine (1 and 5 µM), the contrast of capacitance change for DOPC and DOPC:Chol membrane is higher than that of MPM and DOPC:SM:Chol membrane.

Fig. 2. Representative Nyquist plots (Z′ vs -Z′′) obtained from titration of Miltefosine into contacting solution at (a) DOPC, (b) DOPC:Chol, (c) DOPC:SM:Chol and (d) MPM lipid bilayers suspended across gold microcavity array electrodes. The experiments were carried out in a three-electrode cell, where MSLB array is working electrode, Ag/AgCl (1M KCl) is reference, and Pt coiled is counter electrode. The electrolyte solution used was 0.01 M PBS solution (pH 7.4). EIS was recorded over the frequency ranges 0.05 Hz to 10^5 Hz at a DC bias of 0V with an AC amplitude of 10 mV at 22±1°C. In each panel □, ○, △, ▽, ◊ symbols represent EIS data for 0, 1, 5, 10 and 20 µM Miltefosine in the contact solution, and ◁ represent measurement at fresh PBS buffer after exchanging the drug-containing buffer after post-incubation.
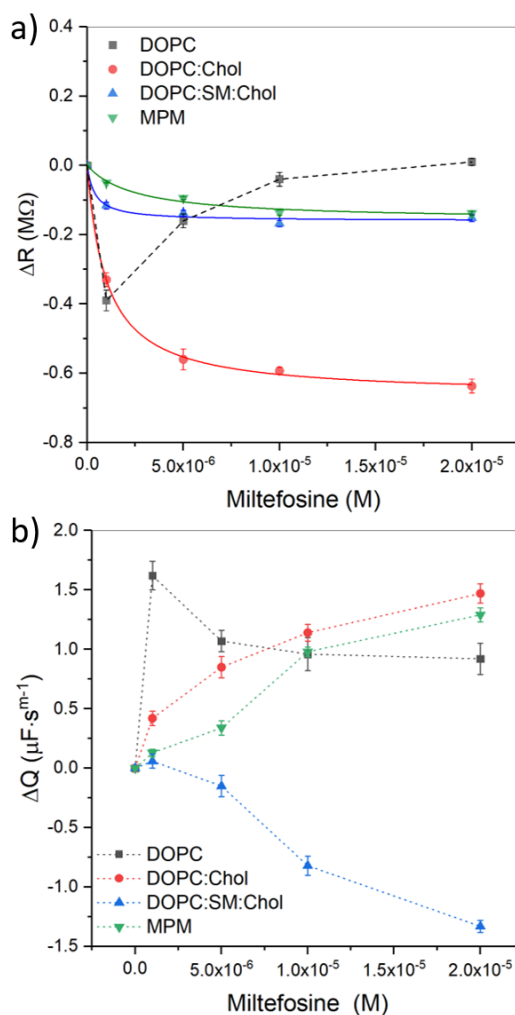

Fig. 3. Relative change in membrane (a) resistance and (b) capacitance obtained from designated lipid composition versus varied Miltefosine concentration. In each panel ■, ●, ▲ and ▼ represent respectively DOPC, DOPC:Chol, DOPC:SM:Chol and MPM membrane composition. In panel (a), the solid lines

extracted. The relative change in resistance and capacitance values are plotted against the concentration of

represent the fit using Eq. (2). The dashed line in each panel is a guide to the eye. Data shown are means ±SD and were measured for each bilayer type in triplicate.

Table 1. Resistance data for different lipid compositions as a function of concentration of Miltefosine. Results presented reflect the relative change (Δ) recorded following drug titration, relative to bilayer prior to drug interaction. The values represent the average value ±S.D. (n=3).

Drug (µM)	ΔR (MΩ)			
	DOPC	DOPC:Chol	DOPC:SM: Chol	MPM
0	0	0	0	0
1	-0.39±0.03	-0.33±0.02	-0.12±0.01	-0.05±0.001
5	-0.16±0.02	-0.56±0.03	-0.14±0.01	-0.09±0.004
10	-0.04±0.02	-0.59±0.01	-0.17±0.01	-0.14±0.007
20	0.01±0.01	-0.64±0.02	-0.15±0.02	-0.19±0.006
FB[a]	-1.17±0.07	-0.76±0.08	0.09±0.05	-0.09±0.03

[a] FB refers to membrane where the drug contacting buffer was exchanged to fresh buffer.

At the end of each titration, the drug-containing buffer was exchanged with fresh PBS to elucidate any irreversible structural impact of Miltefosine on the membranes. In each case, the impedance traces were recorded for the MSLBs in fresh PBS buffer post-incubation with the highest concentration of (20 µM) of miltefosine drug. These data are included in the panel of Fig. 2 (orange symbol), and the relative changes of resistance and capacitance following fresh buffer exchange are tabulated in Tables 1 and 2 respectively, labelled FB.

Table 2. Capacitance from CPE data for different lipid compositions as a function of concentration of Miltefosine. Results presented reflect the relative change (Δ) recorded following drug titration, relative to bilayer before drug interaction. The values represent the average value ±S.D. (n=3).

Drug (µM)	ΔQ (µF·s^{m-1})			
	DOPC	DOPC:Chol	DOPC:SM :Chol	MPM
0	0	0	0	0
1	1.62±0.12	0.42±0.06	0.06±0.03	0.13±0.03
5	1.07±0.09	0.85±0.09	-0.15±0.09	0.34±0.06
10	0.96±0.14	1.14±0.07	-0.82±0.08	0.98±0.04
20	0.92±0.13	1.47±0.08	-1.33±0.05	1.29±0.06
FB[a]	0.00	1.65±0.05	-2.03±0.12	-1.08±0.07

[a] FB refers to membrane where the drug contacting buffer was exchanged for fresh buffer.

On fresh buffer exchange, the capacitance of the DOPC returned to the original value, prior to Miltefosine titration reflected in the identical semicircle regimes in the normalized complex capacitance plot near Y″/ω axis (Fig. S2, SI). However, notably exchanging of 20 µM solution of Miltefosine in PBS for blank buffer reduced the resistance of the membrane further, reflected in the impedance shift towards Z′ (x-axis) in Nyquist plot (Fig. 2a). These effects are reflected in the ΔR and ΔQ data in Table 1 and Table 2 where (ΔQ = 0 µF·s^{m-1}) of DOPC membrane, while resistance decreases significantly to ΔR = -1.17 MΩ.

For DOPC:Chol membrane, after removal of Miltefosine from the contacting solution, the membrane capacitance increased to 1.65±0.05 µF·s^{m-1} indicating membrane thinning, while the resistance decreased (ΔR = -0.76±0.08 MΩ) overall these effects indicate an irreversible impact on the bilayer integrity. Interestingly for DOPC:SM:Chol membrane, buffer exchange resulted in just a small increase in resistance (0.09±0.05 MΩ) but elicited a large decrease in membrane capacitance (ΔQ = -2.03±0.12 µF·s^{m-1}). The same trend in behaviour was observed for the MPM bilayer composition, where a minor change to resistance (-0.09±0.03 MΩ) was accompanied by a large decrease in capacitance (-1.08±0.07 µF·s^{m-1}). As Miltefosine is amphiphilic, it can aggregate into micellar structures above its critical micellar concentration (CMC). Obviously, CMC depends on buffer and ionic strength, and the values reported for Miltefosine CMC correspondingly, vary significantly, e.g. from CMC of ~2.5 µM[57] in distilled water and in 150 mM NaCl, to CMC of 50 µM in PBS buffer.[58] As we focus here on physiological ranges, the effective dose reported for is Miltefosine 2.5-6.5 µM,[22] so we are working with solutions well below the CMC in PBS. Although there is evidence that the DOPC and DOPC/Chol membranes are compromised by the drug, the minimal effect across the range of concentrations on the most biomimetic membranes explored in this work indicates that the drug does not impact the membrane integrity and supports the notion that the mode of action of alkylphospholipid drug is not solely a hemolytic pathway as reported previously.[22,59,60]

3.1. Evaluation of Miltefosine binding using Langmuir isotherm model

In order to provide some quantitative insight into the drug binding to different membrane compositions, ΔR versus Miltefosine concentration data (as shown in Fig. 3a, filled symbols) fit (solid lines, Fig. 3a) iteratively to the empirical Langmuir isotherm model as defined by equation (2). This model applies to non-specific binding[61,62],

$$\Delta R = \frac{\Delta R_{sat}(K_a C)}{1 + K_a C} \qquad (2)$$

where ΔR is the change in membrane resistance, ΔR_{sat} is absorption capacity or saturated binding of the drug, K_a is an empirical association constant and C is the bulk concentration of the drug. The fit parameters to the Langmuir isotherm are provided in Table 3.

As can be seen, as drug concentration increased, a large decrease in resistance values is observed on incubation with 1 μM Miltefosine for DOPC membrane but resistance then recovers again upon addition of further drug. This effect and the fact that binding saturation was not observed within the concentration range explored here, suggests the drug is very permeable toward this simple membrane. Also given the large decrease in resistance post removal of the drug from contacting solution, the DOPC membrane packing seems to be disrupted by the drug. Consequently, the data could not be fit to the Langmuir isotherm model. In contrast, in the presence of cholesterol, for the DOPC:Chol membrane, ΔR decreases systematically and reaches saturation binding. From the Langmuir fit, ΔR_{sat} and K_a are estimated and found to be -0.66±0.006 MΩ and 0.99±0.05 L·μM^{-1} respectively. Note that, the resistance change for cholesterol containing DOPC membrane is greater than for the DOPC-only membrane (cf. Fig. 3a and Table 1) suggesting the mode of interaction of Miltefosine is influenced by cholesterol. Based on the relative direction and magnitude of changes to ΔR and ΔQ for the DOPC and DOPC/Chol membranes, we speculate that the drug permeations efficiently through DOPC membrane but is retained more strongly at the cholesterol containing membrane, mediated presumably by the cholesterol. Our results agree with previous studies that reported cholesterol-induced rapid and strong association of Miltefosine with model membrane.[60] Furthermore, it is believed that the content of unsaturated phospholipid is lower for Miltefosine resistant *Leishmania* than that of wild type. In this context, our results on DOPC:Chol and DOPC-only membrane indicate the latter being unsaturated lipid is highly permeable and susceptible to damage by the drug, but the former is more resistant and a probable target for Miltefosine as previously hypothesized by Rakotomanga et al.[63]

Consistent with this effect, the resistance changes induced by incubating saturation levels of Miltefosine with MSLBs are much smaller for the membranes that contain both SM and Chol. For DOPC:SM:Chol and MPM composition bilayers, the respective ΔR_{sat} were found to be only -0.16±0.008 and -0.15±0.012 MΩ which are similar within the experimental error. Nonetheless, the association constants determined for these compositions, however, are significantly different; estimated as K_a of 2.52±1.01 L·μM^{-1} for DOPC:SM:Chol and 0.39±0.12 L·μM^{-1} for MPM membrane, respectively (Table 3).

As observed, for raft-like ternary lipid mixtures, a closer mimic of eukaryotic membranes, the association is significant. The overall decrease in resistance is relatively small but significant. It is notable that the capacitance values changes on Miltefosine binding and association contrast for DOPC:SM:Chol and for MPM membrane. Like the other compositions capacitance increases for MPM indicating membrane thinning whereas for DOPC:SM:Chol, capacitance decreases. This is suggestive of more membrane permeation in the former 3 cases but primarily interfacial retention of the Miltefosine binding at ternary composition. Membrane retention seems to be mediated by cholesterol given the association constant scales with cholesterol or liquid ordered (L_o) content whereas the most permeable membrane was the DOPC-only. This is consistent with the notion that drug permeation is mediated through liquid disordered regions in a phase separated[64] membrane. Although the detailed mode of action of Miltefosine and related alkylphospholipid analogue is still under debate, some studies have shown their involvement in membrane domain stability, lipid/cholesterol metabolism and apoptosis.[4,65–67] Our observations are also in agreement with a previous study[63] where the accumulation of drugs at the membrane surface is observed to occur at membranes containing cholesterol and saturated phospholipids, that form more ordered structures like SM+Chol phases in Miltefosine resistant *Leishmania* Promastigotes. Furthermore, our results on domain-containing membranes and membrane fluidization properties of Miltefosine are strongly consistent with the earlier reports on molecular dynamics simulations,[68] where Miltefosine was found to interact with lipid rafts and had a higher permeability in loosely organized unsaturated bilayers. In addition, a mild increase in membrane fluidity without altering the biophysical properties of raft domains was observed from fluorescence-based studies.[69]

Finally, given the extensive change to electrical properties of DOPC membrane induced by Miltefosine, a complementary measurement was performed using fluorescence lifetime correlation spectroscopy (FLCS). FLCS measurements were performed at micro pore-suspended membrane at PDMS (Fig. S3, SI) to investigate if Miltefosine induces a change in DOPC membrane fluidity and to confirm that the membrane remained intact on drug incubation. From the FLCS studies, shown in SI, our data importantly confirm that the membrane is not lost on drug treatment. In addition, we observe in the presence of Miltefosine, an increase in lipid diffusivity of 11.8±0.3 μm^2/s from pristine DOPC diffusivity of 9.8±0.2 μm^2/s (i.e., in the absence of Miltefosine), further suggesting the fluidization effect of Miltefosine on the membrane. Our FLCS correlate with a recent report by Chiantia et al.[70]

where Erufosine, an alkylphospholipid analogue increases membrane fluidity at supported lipid model bilayer membrane.

Table 3. Estimated values of ΔR_{sat} and equilibrium association constant, K_a extracted from the Langmuir isotherm model fit during Miltefosine binding to designated lipid compositions. The values represent the average value ±S.D. (n=3).

membrane composition	ΔR_{sat}(MΩ)	K_a(L·µM^{-1})	R^2
DOPC	-	-	-
DOPC:Chol	-0.66±0.006	0.99±0.05	0.99
DOPC:SM:Chol	-0.16±0.008	2.52±1.01	0.98
MPM	-0.15±0.012	0.39±0.12	0.98

For the MPM composition, in spite of Chol/SM content, a low K_a indicates that the interaction is relatively weak. The MPM membrane is composed of negatively charged DOPS (8 mol%) as well as DOPE-a small head group (-NH$_3^+$) lipid (25 mol%) along with DOPC, SM and cholesterol. At neutral pH, although Miltefosine has no net charge it is zwitterionic[17], and in principle, the membrane could experience electrostatic repulsion from the DOPS head group and Miltefosine. Furthermore, DOPE can pack in higher order than that of DOPC due to its small head groups which may reduce the Miltefosine binding. This observation is in line with previous X-ray studies that Miltefosine induced significant structural perturbations to DMPC (phosphatidylcholine head group) multilayers, whereas no relevant effects were observed in DMPE (phosphatidylethanolmine).[27]

4. Conclusions

In summary, we have investigated the impact of Miltefosine, an antileishmanial drug on four microcavity supported lipid membranes of different compositions; single component DOPC, binary DOPC:Chol, ternary raft-like DOPC:SM:Chol and highly physiological fusogenic membrane compositions MPM. In all cases, the drug was observed to change the electrical properties of the membranes over physiological range of Miltefosine by label-free highly sensitive EIS spectroscopy. The extent of change varied strongly with membrane composition.

Comparing the most extreme responses, we observe largest decreases and increases of resistance and capacitance of the membrane at the simple DOPC membrane and weakest interaction at the MPM composition. For cholesterol containing membranes, particularly phase forming compositions, capacitance changes indicate interfacial binding of the drug occurs whereas for DOPC-only membrane the drug seems to permeate strongly with non-Langmuir concentration response and extensive membrane thinning and increased

admittance. Exchanging 20 µM drug for fresh buffer at DOPC elicits irreversible decrease to the membrane resistance but FCS data confirm the membrane remains in place albeit with increased fluidity that is attributed to disruption to membrane packing. Such behaviour is attributed to deep penetration of the drug into the membrane associated with permeation and some evidence of this occurs for all but the ternary domain-forming membrane, which shows both increases in resistance and in particular decreased capacitance on Miltefosine incubation, indicating interfacial binding. Our data offer some insight into the relatively poor uptake of Miltefosine in complex eukaryotic membranes and may offer clues as to how uptake can be improved when the drug is administered with combination therapy using another agent such as amphotericin B or other drugs[71–74]. Overall, the MSLB platform used with EIS is a relatively simple, label free approach to gaining new biophysical insights into drug-membrane interactions and permeation.

Declaration of Competing Interest
The authors declare that there is no conflict of interest.

Appendix A: Supplementary data

List of Scheme, Figure and Table captions

Scheme 1. (a) Schematic representation of microcavity array using polystyrene template method. (b) Illustrates AFM image (*Top*) and line profile analysis (*bottom*) of gold microcavity array. The scale bar in the image was 2 µm. (c) Represents a schematic representation of MSLB (*left*) along with ECM circuit (*right*). Various components of the ECM are; R_{el} : electrolyte resistance, C_{stray}: stray capacitance, R_M: membrane resistance, Q_M: membrane capacitance, R_{array}: cavity array resistance, and Q_{array}: array capacitance. (d) Representative stability plot of DOPC MSLB showing the relative change in resistance versus time. An arrow mark is to show the equilibration time (~2 hr) at which Miltefosine is added to the cell. (e) Chemical structure of hexadecylphosphocholine, Miltefosine.

Fig. 1. a) Nyquist plot and b) frequency normalized complex capacitance plot obtained during impedance measurement at cavity array (open circle, ο) and DOPC MSLB (open square, □). (*inset* in a) Represents Bode plot (frequency vs phase angle,

theta). In each panel, for DOPC MSLB, solid lines represent the fit using ECM, shown in Scheme 1c, and for cavity, the parallel component (R_M and CPE_M) was omitted from the circuit. EIS measurements were performed in 0.01 M PBS buffer within the frequency ranges between 0.05 Hz to 10^5 Hz at 0 V DC bias potential vs Ag/AgCl (1 M KCl) with an AC amplitude of 10 mV at 22±1°C. A three-electrode set-up where gold cavity/MSLB, Ag/AgCl (1M KCl) and Pt coiled served as working, reference and counter electrode respectively.

Fig. 2. Representative Nyquist plots (Z′ vs -Z′′) obtained from titration of Miltefosine into contacting solution at (a) DOPC, (b) DOPC:Chol, (c) DOPC:SM:Chol and (d) MPM lipid bilayers suspended across gold microcavity array electrodes. The experiments were carried out in a three-electrode cell, where MSLB array is working electrode, Ag/AgCl (1M KCl) is reference, and Pt coiled is counter electrode. The electrolyte solution used was 0.01 M PBS solution (pH 7.4). EIS was recorded over the frequency ranges 0.05 Hz to 10^5 Hz at a DC bias of 0V with an AC amplitude of 10 mV at 22±1°C. In each panel □, ○, △, ▽, ◊ symbols represent EIS data for 0, 1, 5, 10 and 20 μM Miltefosine in the contact solution, and ◁ represent measurement at fresh PBS buffer after exchanging the drug-containing buffer after post-incubation.

Fig. 3. Relative change in membrane (a) resistance and (b) capacitance obtained from designated lipid composition versus varied Miltefosine concentration. In each panel ■, ●, ▲ and ▼ represent respectively DOPC, DOPC:Chol, DOPC:SM:Chol and MPM membrane composition. In panel (a), the solid lines represent the fit using Eq. (2). The dashed line in each panel is a guide to the eye. Data shown are means ±SD and were measured for each bilayer type in triplicate.

Table 1. Resistance data for different lipid compositions as a function of concentration of Miltefosine. Results presented reflect the relative change (Δ) recorded following drug titration, relative to bilayer prior to drug interaction. The values represent the average value ±S.D. (n=3).

Table 2. Capacitance from CPE data for different lipid compositions as a function of concentration of Miltefosine. Results presented reflect the relative change (Δ) recorded following drug titration, relative to bilayer before drug interaction. The values represent the average value ±S.D. (n=3).

Table 3. Estimated values of ΔR_{sat} and equilibrium association constant, K_a extracted from the Langmuir isotherm model fit during Miltefosine binding to designated lipid compositions. The values represent the average value ±S.D. (n=3).

Data Availability Statement: The Authors declare that there is no shared data in this work.

References

[1] F. Chappuis, S. Sundar, A. Hailu, H. Ghalib, S. Rijal, R. W. Peeling, J. Alvar, M. Boelaert, *Nat. Rev. Microbiol.* **2007**, *5*, 873–882.
[2] S. L. Croft, S. Sundar, A. H. Fairlamb, *Clin. Microbiol. Rev.* **2006**, *19*, 111–126.
[3] J. de A. Pachioni, J. G. Magalhães, E. J. C. Lima, L. de Moura Bueno, J. F. Barbosa, M. M. de Sá, C. de O. Rangel-Yagui, *J. Pharm. Pharm. Sci.* **2013**, *16*, 742–759.
[4] W. van Blitterswijk, M. Verheij, *Curr. Pharm. Des.* **2008**, *14*, 2061–2074.
[5] S. Sundar, T. K. Jha, C. P. Thakur, J. Engel, H. Sindermann, C. Fischer, K. Junge, A. Bryceson, J. Berman, *N. Engl. J. Med.* **2002**, *347*, 1739–1746.
[6] J. Chakravarty, S. Sundar, *Expert Opin. Pharmacother.* **2019**, *20*, 1251–1265.
[7] S. Sundar, A. Singh, *Ther. Adv. Infect. Dis.* **2016**, *3*, 98–109.
[8] M. Vermeersch, R. I. Da Luz, K. Toté, J. P. Timmermans, P. Cos, L. Maes, *Antimicrob. Agents Chemother.* **2009**, *53*, 3855–3859.
[9] G. Barratt, M. Saint-Pierre-Chazalet, P. Loiseau, *Curr. Drug Metab.* **2009**, *10*, 247–255.
[10] J. R. Luque-Ortega, L. Rivas, *Antimicrob. Agents Chemother.* **2007**, *51*, 1327–1332.
[11] T. P. C. Dorlo, M. Balasegaram, J. H. Beijnen, P. J. de Vries, *J. Antimicrob. Chemother.* **2012**, *67*, 2576–2597.
[12] S. L. Croft, R. A. Neal, W. Pendergast, J. H. Chan, *Biochem. Pharmacol.* **1987**, *36*, 2633–2636.
[13] A. J. Iacano, H. Lewis, J. E. Hazen, H. Andro, J. D. Smith, K. Gulshan, *Sci. Rep.* **2019**, *9*, 11128.
[14] M. Kansy, F. Senner, K. Gubernator, *J. Med. Chem.* **1998**, *41*, 1007–1010.
[15] P. Palit, A. Hazra, A. Maity, R. S. K. Vijayan, P. Manoharan, S. Banerjee, N. B. Mondal, N. Ghoshal, N. Ali, *Antimicrob. Agents Chemother.* **2012**, *56*, 432–445.
[16] A. Reichel, D. J. Begley, *Pharm. Res.* **1998**, *15*, 1270–1274.
[17] I. Rey Gómez-Serranillos, J. Miñones, P. Dynarowicz-Łątka, J. Miñones, O. Conde, *Langmuir* **2004**, *20*, 11414–11421.
[18] J. Miñones, I. Rey Gómez-Serranillos, O. Conde, P. Dynarowicz-Łatka, J. Miñones Trillo, *J. Colloid Interface Sci.* **2006**, *301*, 258–266.
[19] T. T. H. Pham, G. Barratt, J. P. Michel, P. M. Loiseau, M. Saint-Pierre-Chazalet, *Colloids Surfaces B Biointerfaces* **2013**, *106*, 224–233.
[20] C. Ménez, M. Buyse, C. Dugave, R. Farinotti, G. Barratt, *Pharm. Res.* **2007**, *24*, 546–554.
[21] C. Ménez, M. Buyse, R. Farinotti, G. Barratt, *Lipids* **2007**, *42*, 229–240.

[22]   M. Dymond, G. Attard, A. D. Postle, *J. R. Soc. Interface* **2008**, *5*, 1371–1386.

[23]   R. Bilginer, A. Arslan Yildiz, in *Biomim. Lipid Membr. Fundam. Appl. Commer.*, Springer International Publishing, Cham, **2019**, pp. 225–247.

[24]   J. Knobloch, D. K. Suhendro, J. L. Zieleniecki, J. G. Shapter, I. Köper, *Saudi J. Biol. Sci.* **2015**, *22*, 714–8.

[25]   C. Bourgaux, P. Couvreur, *J. Control. Release* **2014**, *190*, 127–138.

[26]   C. Peetla, A. Stine, V. Labhasetwar, *Mol. Pharm.* **2009**, *6*, 1264–1276.

[27]   K. Petit, M. Suwalsky, J. R. Colina, L. F. Aguilar, M. Jemiola-Rzeminska, K. Strzalka, *Biochim. Biophys. Acta - Biomembr.* **2019**, *1861*, 17–25.

[28]   M. Lucio, J. L. F. C. Lima, S. Reis, *Curr. Med. Chem.* **2010**, *17*, 1795–1809.

[29]   A. R. Hillman, K. S. Ryder, E. Madrid, A. W. Burley, R. J. Wiltshire, J. Merotra, M. Grau, S. L. Horswell, A. Glidle, R. M. Dalgliesh, et al., *Faraday Discuss.* **2010**, *145*, 357–379.

[30]   N. J. Yang, M. J. Hinner, *Methods Mol. Biol.* **2015**, *1266*, 29–53.

[31]   N. Kanwa, S. K. De, A. Maity, A. Chakraborty, *Phys. Chem. Chem. Phys.* **2020**, *22*, 3234–3244.

[32]   A. T. Srivatsav, M. Mishra, S. Kapoor, *Biomed Res. Int.* **2018**, *2018*, 6437371.

[33]   H. A. Scheidt, D. Huster, *Acta Pharmacol. Sin.* **2008**, *29*, 35–49.

[34]   Y. Fujino, R. Nakamura, H.-W. Han, I. Yamashita, T. Shimizu, S. Shingubara, T. Ito, *J. Electroanal. Chem.* **2020**, *878*, 114572.

[35]   Y. Nakatani, K. Kawahara, K. Harada, A. Oshima, H. Nakashima, K. Sumitomo, *Jpn. J. Appl. Phys.* **2019**, *58*, SIID06.

[36]   B. Jose, C. T. Mallon, R. J. Forster, C. Blackledge, T. E. Keyes, *Chem. Commun.* **2011**, *47*, 12530.

[37]   P. C. Gufler, D. Pum, U. B. Sleytr, B. Schuster, *Biochim. Biophys. Acta - Biomembr.* **2004**, *1661*, 154–165.

[38]   N. K. Sarangi, A. Patnaik, *ChemPhysChem* **2012**, *13*, 4258–4270.

[39]   T. Fujimoto, I. Parmryd, *Front. cell Dev. Biol.* **2016**, *4*, 155.

[40]   E. T. Castellana, P. S. Cremer, *Surf. Sci. Rep.* **2006**, *61*, 429–444.

[41]   R. Tero, *Materials (Basel).* **2012**, *5*, 2658–2680.

[42]   L. Zhang, S. Granick, *J. Chem. Phys.* **2005**, *123*, 211104.

[43]   Z. Su, J. Jay Leitch, F. Abbasi, R. J. Faragher, A. L. Schwan, J. Lipkowski, *J. Electroanal. Chem.* **2018**, *812*, 213–220.

[44]   N. F. Hussain, A. P. Siegel, Y. Ge, R. Jordan, C. A. Naumann, *Biophys. J.* **2013**, *104*, 2212–2221.

[45]   D. H. Murray, L. K. Tamm, V. Kiessling, *J. Struct. Biol.* **2009**, *168*, 183–189.

[46]   J. Andersson, I. Köper, *Membranes (Basel).* **2016**, *6*, DOI 10.3390/membranes6020030.

[47]   R. Ronen, Y. Kaufman, V. Freger, *J. Memb. Sci.* **2017**, *523*, 247–254.

[48]   M. Vezvaie, C. L. Brosseau, J. Lipkowski, *Electrochim. Acta* **2013**, *110*, 120–132.

[49]   J. Drexler, C. Steinem, *J. Phys. Chem. B* **2003**, *107*, 11245–11254.

[50]   Y. Sun, X. Zang, Y. Sun, L. Wang, Z. Gao, *Chem. Phys. Lipids* **2020**, *228*, 104893.

[51]   S. Ramadurai, N. K. Sarangi, S. Maher, N. MacConnell, A. M. Bond, D. McDaid, D. Flynn, T. E. Keyes, *Langmuir* **2019**, *35*, 8095–8109.

[52]   G. B. Berselli, N. K. Sarangi, S. Ramadurai, P. V. Murphy, T. E. Keyes, *ACS Appl. Bio Mater.* **2019**, *2*, 3404–3417.

[53]   S. Maher, H. Basit, R. J. Forster, T. E. Keyes, *Bioelectrochemistry* **2016**, *112*, 16–23.

[54]   N. K. Sarangi, A. Stalcup, T. E. Keyes, *ChemElectroChem* **2020**, celc.202000818.

[55]   E. Haque, T. J. McIntosh, B. R. Lentz, *Biochemistry* **2001**, *40*, 4340–4348.

[56]   W. K. Chang, W. C. Wimley, P. C. Searson, K. Hristova, M. Merzlyakov, *Biochim. Biophys. Acta - Biomembr.* **2008**, *1778*, 2430–2436.

[57]   M. Rakotomanga, P. M. Loiseau, M. Saint-Pierre-Chazalet, *Biochim. Biophys. Acta - Biomembr.* **2004**, *1661*, 212–218.

[58]   M. B. Barioni, A. P. Ramos, M. E. D. Zaniquelli, A. U. Acuña, A. S. Ito, *Biophys. Chem.* **2015**, *196*, 92–99.

[59]   J. V. Busto, J. Sot, F. M. Goñi, F. Mollinedo, A. Alonso, *Biochim. Biophys. Acta - Biomembr.* **2007**, *1768*, 1855–1860.

[60]   Y. de las M. Zulueta Díaz, M. L. Fanani, *Biochim. Biophys. Acta - Biomembr.* **2017**, *1859*, 1891–1899.

[61]   C. Fenzl, C. Genslein, C. Domonkos, K. A. Edwards, T. Hirsch, A. J. Baeumner, *Analyst* **2016**, *141*, 5265–5273.

[62]   J. C. Soares, A. C. Soares, P. A. R. Pereira, V. D. C. Rodrigues, F. M. Shimizu, M. E. Melendez, C. Scapulatempo Neto, A. L. Carvalho, F. L. Leite, S. A. S. Machado, et al., *Phys. Chem. Chem. Phys.* **2016**, *18*, 8412–8418.

[63]   M. Rakotomanga, M. Saint-Pierre-Chazalet, P. M. Loiseau, *Antimicrob. Agents Chemother.* **2005**, *49*, 2677–2686.

[64]   S. L. Veatch, S. L. Keller, *Biophys. J.* **2003**, *85*, 3074–3083.

[65]   A. H. Van Der Luit, M. Budde, P. Ruurs, M. Verheij, W. J. Van Blitterswijk, *J. Biol. Chem.* **2002**, *277*, 39541–39547.

[66]   M. P. Carrasco, J. M. Jiménez-López, J. L. Segovia, C. Marco, *FEBS J.* **2008**, *275*, 1675–1686.

[67]   P. Ríos-Marco, C. Marco, X. Gálvez, J. M. Jiménez-López, M. P. Carrasco, *Biochim. Biophys. Acta - Biomembr.* **2017**, *1859*, 1657–1667.

[68]   M. Malta De Sá, V. Sresht, C. O. Rangel-Yagui, D. Blankschtein, *Langmuir* **2015**, *31*, 4503–4512.

[69]   B. M. Castro, A. Fedorov, V. Hornillos, J. Delgado, A. U. Acuña, F. Mollinedo, M. Prieto, *J. Phys. Chem. B* **2013**, *117*, 7929–7940.

[70] R. Tzoneva, T. Stoyanova, A. Petrich, D. Popova,
      V. Uzunova, A. Momchilova, S. Chiantia,
      Biomolecules **2020**, *10*, DOI
      10.3390/biom10050802.

[71] J. van Griensven, M. Balasegaram, F. Meheus, J.
      Alvar, L. Lynen, M. Boelaert, *Lancet Infect. Dis.*
      2010, *10*, 184–194.

[72] R. Omollo, N. Alexander, T. Edwards, E. A. G.
      Khalil, B. M. Younis, A. A. Abuzaid, M. Wasunna,
      N. Njoroge, D. Kinoti, G. Kirigi, et al., *Trials* **2011**,
      12, 166.

[73] J. Q. Reimão, D. P. Pita Pedro, A. C. Coelho, *Expert
      Opin. Drug Discov.* **2020**, DOI
      10.1080/17460441.2020.1743674.

[74] N. A. Kasian, V. A. Pashynska, O. V. Vashchenko,
      A. O. Krasnikova, A. Gömöry, M. V. Kosevich, L.
      N. Lisetski, *Mol. Biosyst.* **2014**, *10*, 3155–3162.

Entry of TOC